Wavelength dependence of electron localization of H_2^+ and its isotopomers in the UV-pump-probe scheme*

Shan Xue(薛山)[1,2], Hong-Chuan Du(杜洪川)[1,2,†], Sheng-Jun Yue(岳生俊)[1,2], Hong-Mei Wu(吴红梅)[1,2], and Bi-Tao Hu(胡碧涛)[1,2,‡]

[1] *School of Nuclear Science and Technology, Lanzhou University, Lanzhou* 730000, *China*

[2] *Key Laboratory of Special Function Materials and Structure Design (Ministry of Education), Lanzhou University, Lanzhou* 730000, *China*

(Received 2 October 2016; revised manuscript received 6 December 2016; published online 30 March 2017)

The wavelength dependence of electron localization of H_2^+ and its isotopomers in the ultraviolet pump-probe scheme is investigated by numerically solving the time-dependent Schrödinger equation. By combining with a semiclassical method, an effective analytical formula expressed in the adiabatic representation is established to describe the localization probability with several zero crossings. A stable zone with respect to the laser intensity and carrier envelope phase is found at a relatively long probe wavelength. Finally, the critical probe wavelengths to reach at the stable zone are derived by using the three-dimensional model. Slower nuclear motion of heavier isotopomers leads to a longer critical wavelength.

Keywords: strong field physics, electron localization, molecular dissociation, pump-probe

PACS: 82.53.Eb, 42.50.Hz, 33.80.Rv **DOI:** 10.1088/1674-1056/26/5/058201

1. Introduction

Coherent control of electron and nuclear dynamics with lasers in chemical reactions has attracted a great deal of attention for decades.[1–3] One of the main goals is to steer molecular dissociation into a desired channel selectively by controlling the electron localization, because the gradient of the stark shift can exert a laser induced dipole force on the modification of vibrational motion.[4] With the development of laser technology, in particular the carrier envelope phase (CEP) stabilized few-cycle pulses and sub-femtosecond ultraviolet (UV) pulses,[5–7] several strategies have been proposed to control the electron localization, such as single phase-stabilized few-cycle pulse,[8–10] two-color laser fields,[11–13] UV-pump-infrared (IR)-probe,[14,15] IR-pump-IR-probe,[16,17] attosecond pulse train plus IR fields,[6] and so on.[1–3]

As the simplest molecule, H_2^+ and its isotopomers always work as prototypes and have been studied extensively[8–17] with the aim of extracting the mechanism of electron localization. The key to achieving the localization of H_2^+ is to produce a coherent superposition of channels with different parity. Generally, the lowest states $1s\sigma_g$ and $2p\sigma_u$ are often used because they can be regarded as the bonding and anti-bonding combinations of the 1s atomic orbitals, respectively. In the landmark experiment, Kling *et al.* investigated the dissociation of D_2^+ by utilizing a few-cycle CEP stabilized pulse, and observed that the electron has localized on one of the dissociating nuclei.[9] Lan *et al.* adopted a multi-cycle IR pulse to steer both the electronic and nuclear motion to realize a high localization probability.[12] Liu *et al.* studied the wavelength dependence of the electron localization in the few-cycle pulse scheme, and found that the mid-infrared few-cycle pulse can be used to effectively control the electron localization in molecular dissociation with weak ionization.[10] Unfortunately, in these IR pulse schemes, laser intensities higher than 10^{13} W/cm^2 are often required to obtain significant electron localization. Thus the dissociation ionization and coulomb explosion of the molecular ion become inevitable, so the localization probability decreases naturally in terms of the absolute localization probability of the molecule.

Based on recent study of vibrational quenching of the nuclear wave packet, which moves along the $1s\sigma_g$ potential surface with an initial Frank–Condon distribution after the rapid ionization of H_2, coherent cooling of the molecular vibrational motion can be realized.[4,18] In this case, a resonant UV pulse could be used to pump a part of the wave packet up to the dissociative $2p\sigma_u$ state. Then the electron dynamics can be manipulated by employing either a delayed IR probe pulse[7] or a THz probe pulse.[19] As a result, a higher localization probability up to 99.3% is supposed to be achieved for the THz probe pulse. Moreover, dissociative ionization can be suppressed due to the relatively lower laser intensity (10^{12} W/cm^2). Except for the above advantages, some problems still exist in such a UV-pump-probe scheme. On one hand, the localization probability in the IR probe approach cannot be as high as that in the THz probe approach. On the other hand, the laser intensity required for the THz pulse is

*Project supported by the National Natural Science Foundation of China (Grant Nos. 11404153, 11135002, 11475076, and 11405077) and the Fundamental Research Funds for the Central Universities of China (Grants Nos. lzujbky-2016-29, lzujbky-2016-31, and lzujbky-2016-209).

†Corresponding author. E-mail: duhch@lzu.edu.cn

‡Corresponding author. E-mail: hubt@lzu.edu.cn

© 2017 Chinese Physical Society and IOP Publishing Ltd

still too high to obtain at present. So in order to use these potentially powerful schemes optimally, we theoretically investigate the wavelength dependence of the electron localization in the UV-pump-probe scheme by using the time-dependent Schrödinger equation (TDSE) and a semi-classical method. A simple analytical formula is developed to interpret the electron localization qualitatively and quantitatively, which is justified by varying the wavelength, the CEP, and the intensity of the probe pulse. The rest of the paper is organized as follows. First, the theoretical models are illustrated in Section 2. Then the numerical results and theoretical analysis are presented in Section 3. Finally, we summarize the results in Section 4.

2. Simulation methods

To avoid the extensive calculation of full-dimension, a 1D-TDSE is adopted in this work. After neglecting the center-of-mass motion, it can be written in the non-Born–Oppenheimer approximation (NBOA) as (atomic units are used throughout)

$$\mathrm{i}\frac{\partial}{\partial t}\psi(z,R,t)=\left[H_{\mathrm{n}}(R)+H_{\mathrm{el}}(z,R,t)\right]\psi(z,R,t), \tag{1}$$

where

$$H_{\mathrm{n}}(R)=-\frac{1}{m_{\mathrm{p}}}\frac{\partial}{\partial R^2}+\frac{1}{R}, \tag{2}$$

$$H_{\mathrm{el}}(z,R,t)=-\frac{2m_{\mathrm{p}}+m_{\mathrm{e}}}{4m_{\mathrm{p}}m_{\mathrm{e}}}\frac{\partial}{\partial z^2}+V_{\mathrm{c}}(z,R)+V_{\mathrm{l}}(z,t). \tag{3}$$

The soft-Coulomb potential is $V_{\mathrm{c}}(z,R)=-1/\sqrt{(z-R/2)^2+1}-1/\sqrt{(z+R/2)^2+1}$, which is widely used in the previous studies.[20,21] The laser–molecule interaction is given by $V_{\mathrm{l}}=-(2m_{\mathrm{p}}+2m_{\mathrm{e}})/(2m_{\mathrm{p}}+m_{\mathrm{e}})zE(t)$. Here m_{p} and m_{e} are the nuclear and electronic masses, respectively. R is the internuclear distance, z is the electronic coordinate with respect to the center-of-mass, and $E(t)$ represents the laser electric field.

Since the UV-pump-probe scheme requires quite low laser intensities, only two lowest states ($1s\sigma_{\mathrm{g}}$ and $2p\sigma_{\mathrm{u}}$) are considered. Then the molecular dynamics of H_2^+ can also be described with a simple two-state model.[22] As the time scale of the molecular rotation ranges from several hundred femtoseconds to a few picoseconds, it could be neglected for the femtosecond laser pulse. In the Born–Oppenheimer approximation (BOA), the two-state molecular wave function is expressed as

$$\Psi(z,R,t)=\psi_{\mathrm{g}}(R,t)\,\varphi_{\mathrm{g}}(z,R)+\psi_{\mathrm{u}}(R,t)\,\varphi_{\mathrm{u}}(z,R), \tag{4}$$

where $\varphi_{\mathrm{g}}(z,R)$ and $\varphi_{\mathrm{u}}(z,R)$ are the normalized electronic $1s\sigma_{\mathrm{g}}$ and $2p\sigma_{\mathrm{u}}$ bound states, respectively. $\psi_{\mathrm{g}}(R,t)$ and $\psi_{\mathrm{u}}(R,t)$ are the corresponding time-dependent nuclear wave packets propagating along the $1s\sigma_{\mathrm{g}}$ ($V_{\mathrm{g}}(R)$) and $2p\sigma_{\mathrm{u}}$ ($V_{\mathrm{u}}(R)$) potential surfaces, which can be calculated by the two-state TDSE

$$\mathrm{i}\frac{\partial}{\partial t}\begin{pmatrix}\psi_{\mathrm{g}}(R,t)\\ \psi_{\mathrm{u}}(R,t)\end{pmatrix}=\begin{pmatrix}T_R+V_{\mathrm{g}}(R) & -u(R)E(t)\\ -u(R)E(t) & T_R+V_{\mathrm{u}}(R)\end{pmatrix}\begin{pmatrix}\psi_{\mathrm{g}}(R,t)\\ \psi_{\mathrm{u}}(R,t)\end{pmatrix}. \tag{5}$$

Here $T_R=-\frac{1}{m_{\mathrm{u}}}\frac{\partial^2}{\partial R^2}$ is the nuclear kinetic energy operator. $u(R)=R/2$ represents the dipole coupling between these two states.[23] The initial state is the vibrational ground state of $V_{\mathrm{g}}(R)$. During the propagation, the nuclear wave functions satisfy $\langle\psi_{\mathrm{g}}\mid\psi_{\mathrm{g}}\rangle+\langle\psi_{\mathrm{u}}\mid\psi_{\mathrm{u}}\rangle=1$.

In our calculation, the laser pulse is assumed to be linearly polarized along the molecular orientation, otherwise dissociative π orbitals will be excited.[24] Then the electric field can be expressed as

$$\begin{aligned}E(t)\;=\;&E_{\mathrm{pump}}\sin(\omega_{\mathrm{pump}}t)\exp(-2\ln 2((t-80)/\tau_{\mathrm{pump}})^2)\\&+E_{\mathrm{probe}}\sin(\omega_{\mathrm{probe}}t+\varphi)f_{\mathrm{probe}}(t),\end{aligned} \tag{6}$$

where φ is the CEP of the probe pulse, and the subscripts pump and probe denote the two laser field components. Since the equilibrium internuclear distance is 2.6 a.u. in our simulation, then the frequency ω_{pump} of one-photon transition to the $2p\sigma_{\mathrm{u}}$ state is 0.33 a.u. (138 nm). The UV pulse duration τ_{pump} as short as 1 fs is chosen to excite an initial compact dissociative wave packet. Such short duration can be generated with the high-order harmonic (HHG) technique.[25,26] The probe pulse profile $f_{\mathrm{probe}}(t)$ has a trapezoidal shape started from $t=-t_0$ with one-cycle turn-on and turn-off, and a 30 fs plateau, where t_0 is the period of the probe wavelength.

The initial ground states for Eqs. (1) and (5) are obtained by the evolution of the field-free Schrödinger equation in imaginary time. Then the TDSE is numerically solved using the split-operator method.[27] A mask function is multiplied at each time step to avoid spurious reflections from the spatial boundaries. By subtracting the vibrational bound states, we define a dissociative wave packet (DWP) $\psi_{\mathrm{DWP}}(R,t)=\psi_{\mathrm{g}}(R,t)+\psi_{\mathrm{u}}(R,t)-\sum_{n=1}^{n=20}\langle v_n(R)/\psi_{\mathrm{g}}(R,t)\rangle v_n(R)$, where v_n is the vibrational bound state. Then, at the end of the laser pulse, the electron localization probability can be expressed by a localized asymmetric parameter (LAP)

$$A=\frac{\langle\psi_{\mathrm{DWP}}/\psi_{\mathrm{DWP}}\rangle_{z>0}-\langle\psi_{\mathrm{DWP}}/\psi_{\mathrm{DWP}}\rangle_{z<0}}{\langle\psi_{\mathrm{DWP}}/\psi_{\mathrm{DWP}}\rangle_{z>0}+\langle\psi_{\mathrm{DWP}}/\psi_{\mathrm{DWP}}\rangle_{z<0}}. \tag{7}$$

3. Results and discussion

To investigate the probe wavelength dependence of the electron localization, the intensity of the UV pulse is set to be 3.5×10^{12} W/cm^2. Such a high intensity will pump about 9.89% wave packet onto the dissociative $2p\sigma_{\mathrm{u}}$ state. We emphasize that the intensity of the UV pulse can be varied from 10^{10} W/cm^2 to 10^{12} W/cm^2: it only determines the probability of resonant excitation onto the $2p\sigma_{\mathrm{u}}$ state, but not the following dissociative electron dynamics. Using Eq. (7), we respectively calculate the LAP in both the NBOA model and the two-state BOA model when it goes stable. Figure 1 depicts

the distinct difference of the electron localization at four different probe pulses with the wavelengths of 800 nm, 1200 nm, 2000 nm, and 4000 nm by scanning the CEP and the electric field intensity of the probe pulse. One can see that the two models show satisfactory agreements, meaning that the two-state model is adequate enough to describe the UV-pump-probe scheme. However, if the probe intensity continues to increase, more molecular orbitals will be included, which will lead to the failure of the two-state model. From Fig. 1, two distinct conclusions can be derived. First, the probe pulse with longer wavelength manifests a better degree of electron localization. Second, for a longer probe wavelength, the LAP will reach a stable zone in which A is not sensitive to some ranges of the field intensity (0.005 a.u.–0.03 a.u.) and the CEP (0–0.5π, π–1.5π). We have also checked the calculations with different pulse profiles, i.e., Gaussian profile and different turn-on and turn-off trapezoidal profiles, and find that the LAP does not depend sensitively on the profile as long as the profile varies smoothly in the intermediate region, so the pulse duration should be much longer than that of the trapezoidal case. The intermediate region is shown as the grey region in Fig. 2.

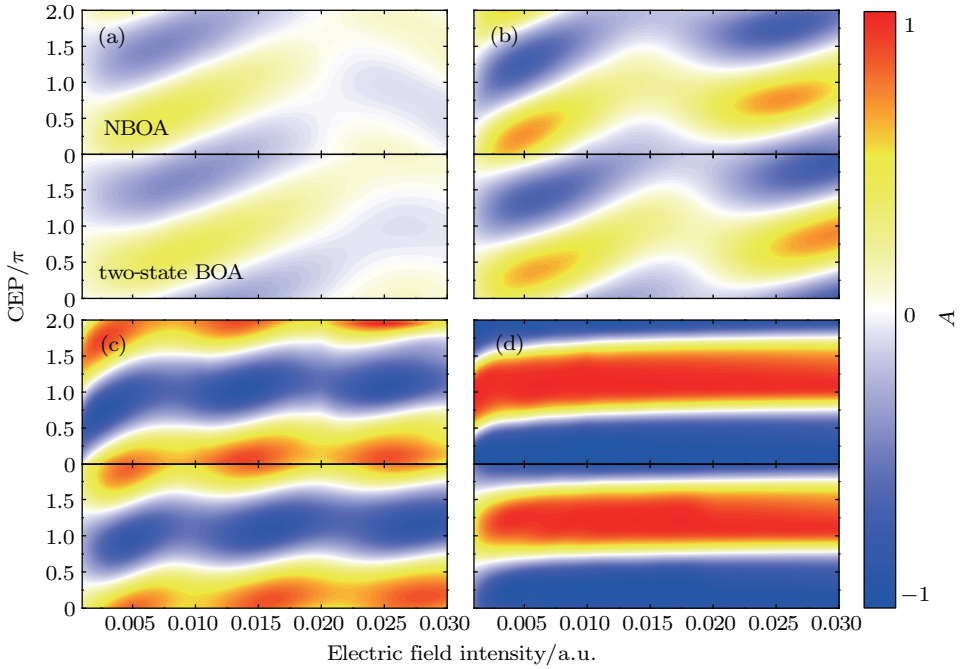


Fig. 1. (color online) Localized asymmetric parameter A calculated using Eq. (7) in both NBOA-TDSE ((a), (b)) and two-state BOA-TDSE ((c), (d)) as a function of the CEP and the electric field intensity of the probe pulses with different wavelengths: (a) 800 nm, (b) 1200 nm, (c) 2000 nm, and (d) 4000 nm.

3.1. Analytical method using quasi-static states

In order to gain deeper insight into the physical mechanism behind these novel phenomena, we develop an analytical formula by expressing the LAP in the adiabatic representation with the help of a semi-classical method. To begin with, the nuclear wave packet for electrons located on the left $\psi_{\rm l}$ and right $\psi_{\rm r}$ nuclei can be expressed as

$$\begin{aligned}\psi_{\rm l} &= \frac{1}{\sqrt{2}}(\psi_{\rm g}+\psi_{\rm u}),\\ \psi_{\rm r} &= \frac{1}{\sqrt{2}}(\psi_{\rm g}-\psi_{\rm u}),\end{aligned} \tag{8}$$

where $\psi_{\rm g}$ is treated by subtracting out the bound state and then the sum of the populations is normalized to unity (this processing method will be used in the following unless otherwise stated). Then the LAP reads

$$A = \frac{\langle\psi_{\rm l}|\psi_{\rm l}\rangle - \langle\psi_{\rm r}|\psi_{\rm r}\rangle}{\langle\psi_{\rm l}|\psi_{\rm l}\rangle + \langle\psi_{\rm r}|\psi_{\rm r}\rangle}.$$

This equation can be quite accurate for large enough internuclear distance. On the other hand, the adiabatic or laser-dressed quasi-static nuclear wave functions $\psi_{\pm}$ can be obtained by diagonalizing the molecular Hamilton matrix

$$\begin{aligned}\psi_{+} &= \cos\theta\,\psi_{\rm g}+\sin\theta\,\psi_{\rm u},\\ \psi_{-} &= -\sin\theta\,\psi_{\rm g}+\cos\theta\,\psi_{\rm u},\end{aligned} \tag{9}$$

where θ satisfies $\tan 2\theta = \frac{2u(R)E(t)}{\omega_{\rm gu}(R)}$ with $\omega_{\rm gu}(R) = V_{\rm u} - V_{\rm g}$; and the corresponding dressed potential surfaces are

$$\begin{aligned}V_{\pm}(R) = \frac{1}{2}\Big[&V_{\rm g}(R)+V_{\rm u}(R)\\ &\pm\sqrt{(V_{\rm g}(R)-V_{\rm u}(R))^2+4u(R)^2E(t)^2}\Big].\end{aligned}$$

By combining Eq. (8) with Eq. (9), one deduces that $\psi_{\rm l,r} = [(\cos\theta \mp \sin\theta)\psi_{+} \mp (\cos\theta \pm \sin\theta)\psi_{-}]/\sqrt{2}$. Then, by integrating the localized nuclear wave function, the LAP can be

expressed in the quasi-static states representation as

$$A = \langle\psi_-|\sin 2\theta\,|\psi_-\rangle - \langle\psi_+|\sin 2\theta\,|\psi_+\rangle - 2\mathrm{Re}(\langle\psi_+|\cos 2\theta\,|\psi_-\rangle). \quad (10)$$

To further simplify Eq. (10), we employ the semi-classical method[28,29] to describe the dissociative process, in which the nuclear motion is treated as an ensemble of classical trajectories moving along the time-dependent adiabatic potential surface. In the UV-pump-probe scheme, a compact dissociative wave packet is initially stimulated by the short UV pulse. With only slight wave packet spreading during the dissociation, the nuclear trajectories can be described mainly by the time-dependent averaged internuclear distance $\bar{R}$. Then θ is just a function of $\bar{R}$ and can be taken out from the integral of Eq. (10). At the beginning of the interaction, the internuclear separation is small, so $u(\bar{R}) \ll \omega_{\mathrm{gu}}(\bar{R})$, which leads to $\theta \approx 0$. Thus $\sin 2\theta \approx 0$ and $\psi_+ \approx \psi_{\mathrm{g}} \approx 0$, meaning that the LAP is zero at the initial time. However, as the molecule dissociates, $u(\bar{R})$ increases linearly and $\omega_{\mathrm{gu}}(\bar{R})$ decreases exponentially, θ tends to become $\pm\pi/4$. Finally, the LAP can be expressed in a simple formula as

$$A \approx \begin{cases} \langle\psi_-|\psi_-\rangle - \langle\psi_+|\psi_+\rangle, & E(t) > 0, \\ \langle\psi_+|\psi_+\rangle - \langle\psi_-|\psi_-\rangle, & E(t) < 0. \end{cases} \quad (11)$$

The sign changes around the zero-cross points of the laser field ($(E(t) = 0)$; the population of the quasi-static states will hop entirely from one to another when avoided crossings occur at these points,[9,30,31] notably, leaving the existing electron localization intact. In brief, for a multi-cycle probe pulse, LAP changes from 0 to a constant when $\bar{R}$ is large enough. Most of all, the greater the population difference of $\psi_\pm$ is, the more significant the electron localization will be. Combining with the Landau–Zener formula[28,32]

$$P(R,t) = \exp\left(-\frac{\pi\omega_{\mathrm{gu}}(\bar{R})^2}{4\omega_{\mathrm{probe}}u(\bar{R})E_{\mathrm{probe}}f_{\mathrm{probe}}(t)}\right), \quad (12)$$

which indicates the transition probability of the adiabatic states at the zero crossings ($E(t) = 0$), one could predict the localization probability quantitatively in principle. This adiabatic representation is more instructive than the common non-adiabatic representation, because the time-dependent process can be simplified into quantitative analyses of several zero crossings.

3.2. Probe wavelength dependence

In Fig. 2, we respectively present the time-dependent process for shorter (800 nm) and longer (4000 nm) probe wavelengths. The laser parameters $E_0 = 0.007$ a.u., $\varphi = 0.5\pi$ are chosen for 800 nm (left column of Fig. 2) and $E_0 = 0.01$ a.u., $\varphi = 1.2\pi$ for 4000 nm (right column of Fig. 2), at which the LAPs reach their maxima. For simplicity, we only focus on the electron localization around the left nucleus, and vice versa. Grey color is calculated by Eq. (12) in which the adiabatic transition probability satisfies $0.1\% < P(t) < 99.9\%$. It indicates an intermediate region in which the dynamic process is neither "adiabatic" (weak coupling with the external field at small internuclear distance) nor "diabatic" (strong coupling with the external field at large internuclear distance), and an effective duration for the electron to transfer to determine the final LAP. As can be seen from Figs. 2(a)–2(d), the population varies symmetrically of the two adiabatic states, which shares the same mechanism of the former work;[33] and the absolute population differences of ψ_+ and ψ_- tend to be equal to the LAPs at latter time, which verifies the correctness and effectiveness of Eq. (11). On further examination, it is found that the LAPs drop periodically beyond the intermediate region. This comes from the bond hardening induced by the probe pulse; and will vanish after the pulse is over with negligible dissociation.[34] Firstly, we focus on the right column of Fig. 2 for the 4000 nm probe pulse. As shown in Fig. 2(f), the only zero-cross position ($E(t) = 0$) in the intermediate region locates at a high transition probability. Hence, when the dressed wave packets encounter this point, they will transfer significantly from each other, then remain unchanged until reaching the next zero crossing. Beyond the intermediate region, the populations undergo a complete reversal at the zero crossings. Physically, this means that the electron stays on a certain nucleus and can no longer move to another. In this situation, we could manipulate the degree of electron localization through controlling the transition of the two dressed states. In other words, by adjusting the CEP of the probe pulse, one could change the zero-cross location in the intermediate region and then realize the controlling of the electron localization.

In contrast, for the 800 nm probe pulse shown in the left column of Fig. 2, a more complex transition process takes place; the final LAP is quite small. For better understanding, we deduce the BOA-TDSE of the quasi-static states by inserting Eq. (9) into the Schrödinger equation

$$\mathrm{i}\frac{\partial}{\partial t}\begin{pmatrix}\psi_+(R,t)\\ \psi_-(R,t)\end{pmatrix} = \begin{pmatrix} T_R+V_+(R) & \mathrm{i}\dot{\theta}(R,t) \\ -\mathrm{i}\dot{\theta}(R,t) & T_R+V_-(R)\end{pmatrix}\begin{pmatrix}\psi_+(R,t)\\ \psi_-(R,t)\end{pmatrix}, \quad (13)$$

where

$$\dot{\theta}(R,t) = \frac{u(R)\dot{E}(t)\omega_{\mathrm{gu}}(R)}{\omega_{\mathrm{gu}}^2(R)+4u^2(R)E^2(t)}$$

acts as the amplitude coupling term between the adiabatic states, and tends to be infinity at the zero crossings as R increases. Then the complexity of transition can be explained in two points. Firstly, as shown in Fig. 2(a), in the intermediate region, some wave packets will be transferred from ψ_+ to ψ_- state after the first transition point t^*; then the two states overlap with each other in both coordinate and momentum spaces

until encountering the next zero crossing $t^{**} = t^* + \pi/\omega_{\text{probe}}$. Therefore, the accumulated phase difference between the two states will generate an interference effect during the following transitions. This effect is highly complex and has been neglected in Eq. (12). Secondly, $\dot{\theta}(R,t)$ in Fig. 2(e) shows smaller and wider humps and undulates periodically following the electric field in the intermediate region. Thus the transitions will occur not just at the zero crossings but over wider time ranges, leading to an inaccurate description of Eq. (12).

Since the effective transition of the adiabatic states only happens at the zero crossings ($E(t) = 0$) in the intermediate region, beyond this region, the transition probability will be either 0 or 1. So multiple transitions will make the population of the two states become close to each other. Therefore we conclude that, in general, the more zero crossings ($E(t) = 0$) the intermediate region contains, the smaller difference the population of $\psi_\pm$ will be, namely, smaller LAP value according to Eq. (11), even though there exists a complex interference effect. So in order to obtain a high localization probability, one should adopt a relatively long probe wavelength to guarantee that only one or no zero crossing appears in the intermediate region, which means that the half optical period should be equal to or longer than the time duration of the region τ_i, namely, $\tau_i \omega_{\text{probe}}/\pi \leq 1$.

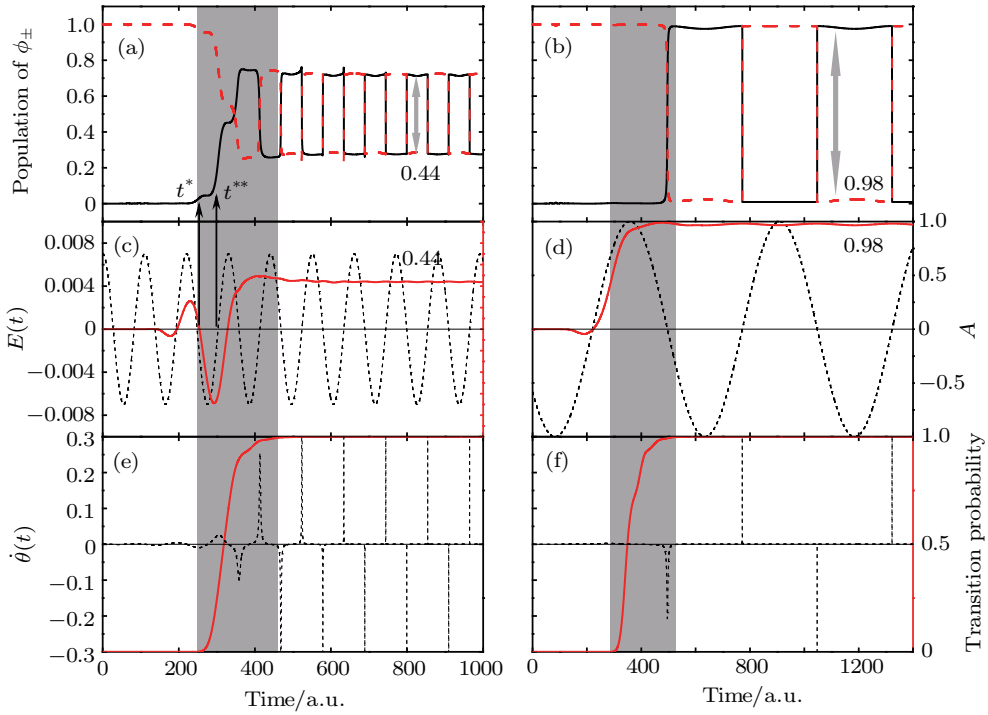


Fig. 2. (color online) (a), (b) The time-dependent population of ψ_+ (black solid lines) and ψ_- (red dashed lines). (c), (d) The LAPs (red solid lines) are calculated using Eq. (7). (e), (f) $\dot{\theta}$ (black dotted lines) and the transition probability (red solid lines) of $\psi_\pm$ are derived from the main nuclear trajectory $\bar{R}$. The electric fields $E(t)$ (black dotted lines) are also given in panels (c) and (d) for clear identification of the zero crossings. The grey region covers the value of the transition probability from 0.1% to 99.9% calculated by Eq. (12). Panels (a), (c), and (e) are for 800 nm, and panels (b), (d), and (f) are for 4000 nm.

3.3. Stable zone

An interesting point worth noting in Fig. 1 is that, for the long wavelength, there exists a stable zone, in which the electron localization appears to be insensitive to the probe laser intensity and the CEP. First we focus on the localization stability on laser intensity. On one hand, the transition of adiabatic states always happens during a small interval of high $\dot{\theta}$ values. In this respect, a probe pulse with small optical frequency ω_{probe} can significantly shrink the intervals' width near the zero-cross points due to the existing of $\dot{E}$ in the numerator of $\dot{\theta}$; whereas the laser intensity plays a minor role on the intervals' width. On the other hand, there will be only one or even no zero crossing included in the intermediate region for the long probe wavelength, i.e., $\tau_i \omega_{\text{probe}}/\pi \leq 1$, so that the transition occurs at most once without any interference effect. Based on these two points, the transition between adiabatic states will follow Eq. (12) quite precisely at exactly the zero crossings no matter how the laser intensity changes. Above all, along the time coordinate, the intermediate region shifts slowly for multi-cycle pulse as the laser intensity increases; that is to say, the transition probability almost keeps unchanged at certain zero crossings. Therefore, the LAP will be stable against the laser intensity for the long probe wavelength.

Whereas for the probe pulse with a short wavelength, the transition interval defined by $\dot{\theta}$ can be much extended; then the laser intensity plays a more important role during the transition process. The larger the intensity is, the more significant the undulation of $\dot{\theta}$ will be in the intermediate region. Then

the resulting successive transition will make the interference effect apparent, resulting in the instability of the electron localization against the probe intensity.

In the aspect of localization stability on the CEP, the half optical period of the probe pulse should be much longer than the time duration of the intermediate transition region τ_i, i.e., $\tau_i \omega_{probe}/\pi \ll 1$. Then the probability of finding a zero crossing in the intermediate region is quite low. In other words, the transition of adiabatic states happens with a great probability of either 0 or 1, leaving $|A| = |\langle\psi_+/\psi_+\rangle - \langle\psi_-/\psi_-\rangle| \approx 1$. If the probe wavelength becomes longer, one should expect that the stable zone will be more broadened in terms of the CEP, and the LAP will be either 1 or -1.

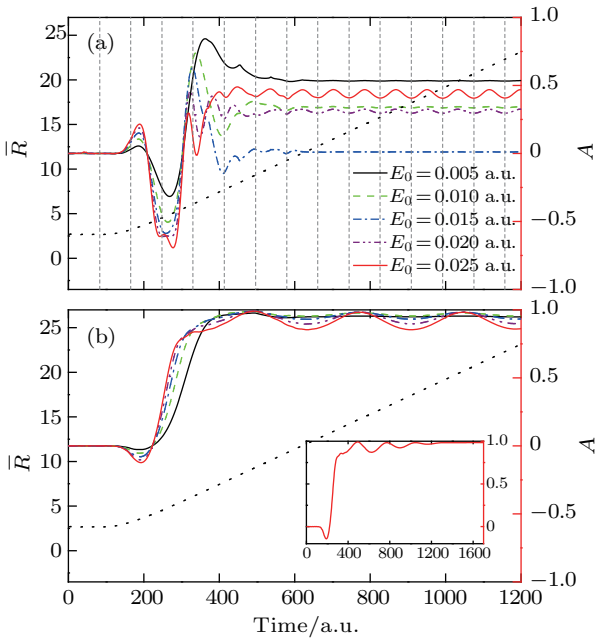


Fig. 3. (color online) The time-dependent internuclear distance $\bar{R}$ is presented as the black dot line. The time-dependent LAP A is calculated in the two-state BOA-TDSE at different electric field intensities for probe wavelengths of (a) 1200 nm and (b) 4000 nm. The vertical dash lines indicate the time at which the electric field reaches its maximum absolute values for a 1200 nm pulse. The inset in panel (b) shows the LAP evolution with an envelope of 15 fs plateau and 22 fs turn-off at $E_0 = 0.025$ a.u.

For better understanding the stable zone, we analyze the localized process from another perspective, namely, the electron tunneling through the internuclear potential barrier. In Fig. 3, we provide the time-dependent averaged internuclear distance $\bar{R}$ and the LAP for the probe wavelengths of 1200 nm ($\phi = 0.5\pi$) and 4000 nm ($\phi = 1.2\pi$) at different laser intensities. The periodical drops of the LAP after 500 a.u. at higher intensities come from the bond hardening of the undissociated $1s\sigma_g$ state, and locate exactly at the time of the maximum electric field (vertical dash line).[34] It will be vanished by using a long pulse tail, which can be seen from the inset of Fig. 3(b). So we take the maximum absolute value of A after 500 a.u. as the final LAP. For the 4000 nm pulse, the LAP increases rapidly to unity near 300 a.u., and higher intensity can only shorten the tunneling duration but basically not change the localization probability. This is because a probe pulse with long wavelength will provide enough time for the electron to transfer from one nuclei to another, making the tunneling an adiabatic quasi-static process. When the sign of the electric field changes after a half-cycle, $\bar{R}$ has increased to a much longer distance ($\sim$ 10 a.u.). Although the laser intensity increases, the tunneling probability still decreases exponentially, leaving the LAP unchanged. So this is the reason for the existance of the stable zone at the longer probe wavelength. Whereas for the 1200 nm probe wavelength shown in Fig. 3(a), half an optical period will not be enough for the electron to transfer. Then the non-adiabatic tunneling will dominate the electron transfer through the internuclear potential barrier. At lower intensity (solid thin black line), tunneling mainly happens around 330 a.u. When time goes to 410 a.u., $\bar{R}$ increases to 7.5 a.u., then the electric field will not be strong enough to transfer plenty of the electronic wave packet to the right side. So the electron locates almost around the left nucleus. As the laser intensity increases (dash dot blue line), tunneling through the internuclear potential barrier could happen earlier, and a new channel (tunneling through larger $\bar{R}$) will be opened. These correspond to the electron moving toward the right nucleus around 240 a.u. and 370 a.u., and will significantly offset the tunneling to the left nucleus around 300 a.u.. So the final LAP is suppressed. If the intensity continues to increase (solid thick red line), another non-adiabatic phenomenon occurs. The LAP starts to shake at a high value near 330 a.u. This can be attributed to the rapid change of the internuclear potential barrier at such a high intensity, which causes a back scattering of the wave packet at the large internuclear distance, i.e., $\bar{R} = 6$ a.u. Finally the electron will be located around the left nucleus, leaving the LAP at a high value again. The same mechanism can also occur in other short probe wavelength cases, in which the complex non-adiabatic tunneling will lead to a periodic oscillation of the LAP as the intensity increases. Actually, these two physical pictures, the adiabatic states representation and the tunneling representation, both explain the electron localization quite well. The latter can be more intuitive whereas the former provides a quantitative description of the LAP. Moreover, the intermediate region shown in Fig. 2 represents the effective tunneling time of the internuclear barrier in the tunneling representation.

3.4. Isotopic effect

Next, we investigate the isotopic effect of electron localization in the UV-pump-probe scheme. Taking T_2^+ for example, we show the degree of electron localization at four different probe wavelengths in Fig. 4. One can see periodical oscillation and a smaller value of the LAP compared with that

of H_2^+ for 4000 nm. However, the stability reemerges at the much longer wavelength of 8000 nm, meaning that the electron localization is independent of the laser intensity and the CEP. According to Eq. (12), slow motion of the heavier nuclei, namely, gradual variation of $\bar{R}$, will lead to a broadened duration of the intermediate region, meaning that more zero crossings will be included in the region compared with that of H_2^+ for the same probe wavelength. Thus the localization probability decreases and the interference effect becomes inevitable due to multiple transitions. However with increasing wavelength, less zero-cross points will be contained in the intermediate region. As a result, the stable zone reappears at a much longer probe wavelength.

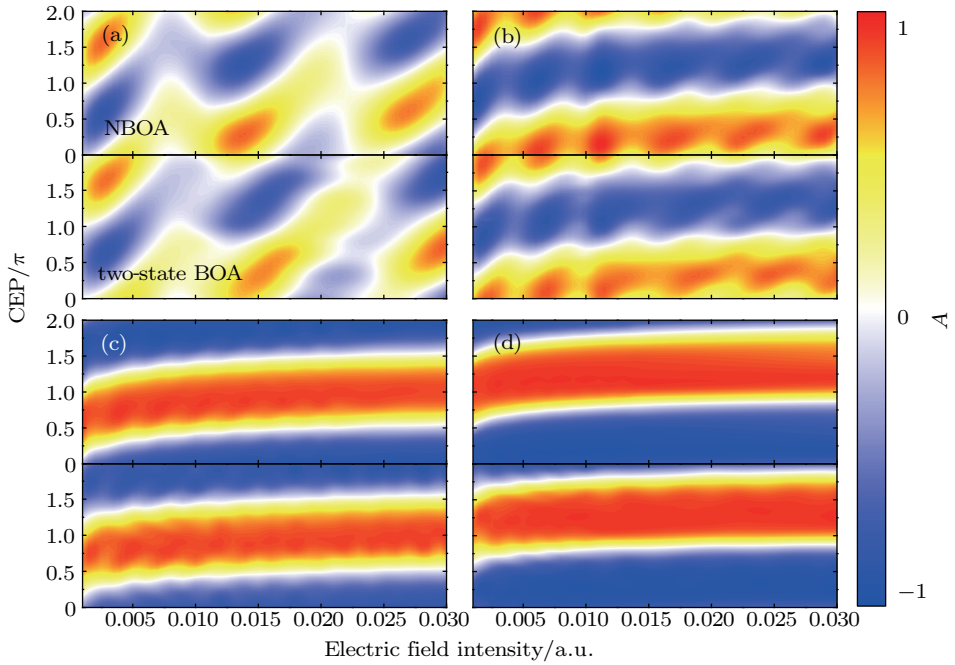


Fig. 4. (color online) For T_2^+, the LAP calculated using Eq. (7) in both the NBOA-TDSE ((a), (b)) and the two-state BOA-TDSE ((c), (d)) as a function of the CEP and the electric field intensity of the probe pulse with different wavelengths: (a) 2000 nm, (b) 4000 nm, (c) 6000 nm, and (d) 8000 nm.

From the view of tunneling through the internuclear potential barrier, a new tunneling channel (tunneling through larger $\bar{R}$) can still be opened for the 4000 nm wavelength when the laser intensity increases after the main tunneling. Then non-adiabatic effects take place, leading to the periodical oscillation of the LAP against the laser intensity. This is because the internuclear distance increases a little for heavier nuclei during a half-cycle. In order to overcome the opening of new tunneling channels, a longer wavelength (8000 nm) should be adopted. Therefore at the time half-cycle after the main tunneling, $\bar{R}$ will be separated large enough to prevent another tunneling, then the LAP will be stable again. This shares the same mechanism as shown in Fig. 3.

In the stable zone, the LAP can be calculated with a quantitative formula$A = 1 - 2P(\bar{R}_0, t_0)(E(t) > 0)$, where $\bar{R}_0$ is the averaged internuclear separation at exactly the zero-cross time t_0 in the intermediate region. In Fig. 5(a), 4000 nm probe wavelength with $E_0 = 0.01$ a.u. is adopted for H_2^+, and 8000 nm probe wavelength with $E_0 = 0.01$ a.u. for T_2^+. One can see that the analytical results agree well with the simulated results. Therefore, the analytical method established in this paper is reliable and can be used to evaluate the electron localization probability quantitatively in the stable zone.

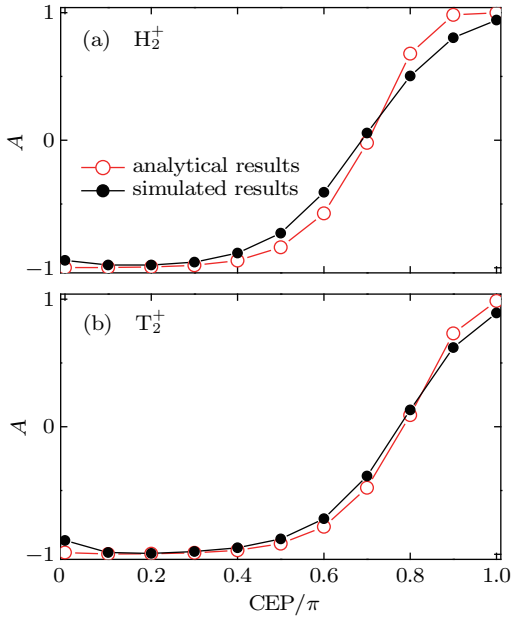


Fig. 5. (color online) (a), (b) The LAP in the stable zone ($E_0 = 0.01$ a.u.) obtained by the analytical method (red hollow circle) and the two-state BOA-TDSE using Eq. (7) (black solid cycle). Probe wavelengths 4000 nm and 8000 nm are selected for H_2^+ (a) and T_2^+ (b), respectively.

In the end, we calculate the LAP in the three-dimensional model to verify our conclusion. Within this model, the Hamiltonian is given as

$$H_0 = -\frac{1}{m_p}\frac{\partial^2}{\partial R^2} - \frac{2m_p+m_e}{4m_p m_e}\left(\frac{\partial^2}{\partial z^2}+\frac{\partial^2}{\partial \rho^2}+\frac{1}{\rho}\frac{\partial}{\partial \rho}\right) + \frac{1}{\sqrt{R^2+\beta}} - \frac{1}{\sqrt{(z-R/2)^2+\rho^2+\alpha}} - \frac{1}{\sqrt{(z+R/2)^2+\rho^2+\alpha}}. \quad (14)$$

The soft parameters $\alpha = 0.0109$ and $\beta = 0.1$ have been chosen to yield the experimental ground state energy and equilibrium distance of -0.6028 and 2.0 a.u., respectively.[15] The frequency of the pump pulse is chosen to be 0.43 a.u. to match the one-photon transition energy to the $2p\sigma_u$ state. The results shown in Fig. 6 indicate that the stable zone can still be found in the realistic model of hydrogen molecular ion and its isotopomers. The discrepancy of the CEP patterns of Figs. 4 and 6 comes from the different TDSE model used here. To evaluate the critical probe wavelength λ_c at which the LAP just reaches at the stable zone, according to the inequality $\tau_i \omega_{probe}/\pi \ll 1$, we calculate the maximum time duration ($0.1\% \le P \le 99.9\%$) of the intermediate region τ_i at the probe intensity range 0.01–0.03 a.u. using Eq. (12). Then $\lambda_c = 2c\tau_i$ with c the speed of light. For H_2^+, λ_c is about 3000 nm, and for T_2^+, λ_c is about 8000 nm, which is much longer than that of H_2^+. Generally speaking, λ_c is inversely proportional to the velocity of $\bar{R}$. Heavier nuclei can largely reduce the nuclear motion, so a longer λ_c is required to reach at the stable zone. Besides, figures 6(d) and 6(h) show that the stable zone will be enlarged against the CEP at a much longer probe wavelength, which has been predicted in Subsection 3.3. The laser intensity of the pump pulse will only determine the pump probability to the dissociative $2p\sigma_u$ state, but hardly the following trajectory of $\bar{R}$, so the localization process will not be influenced by the pump intensity.

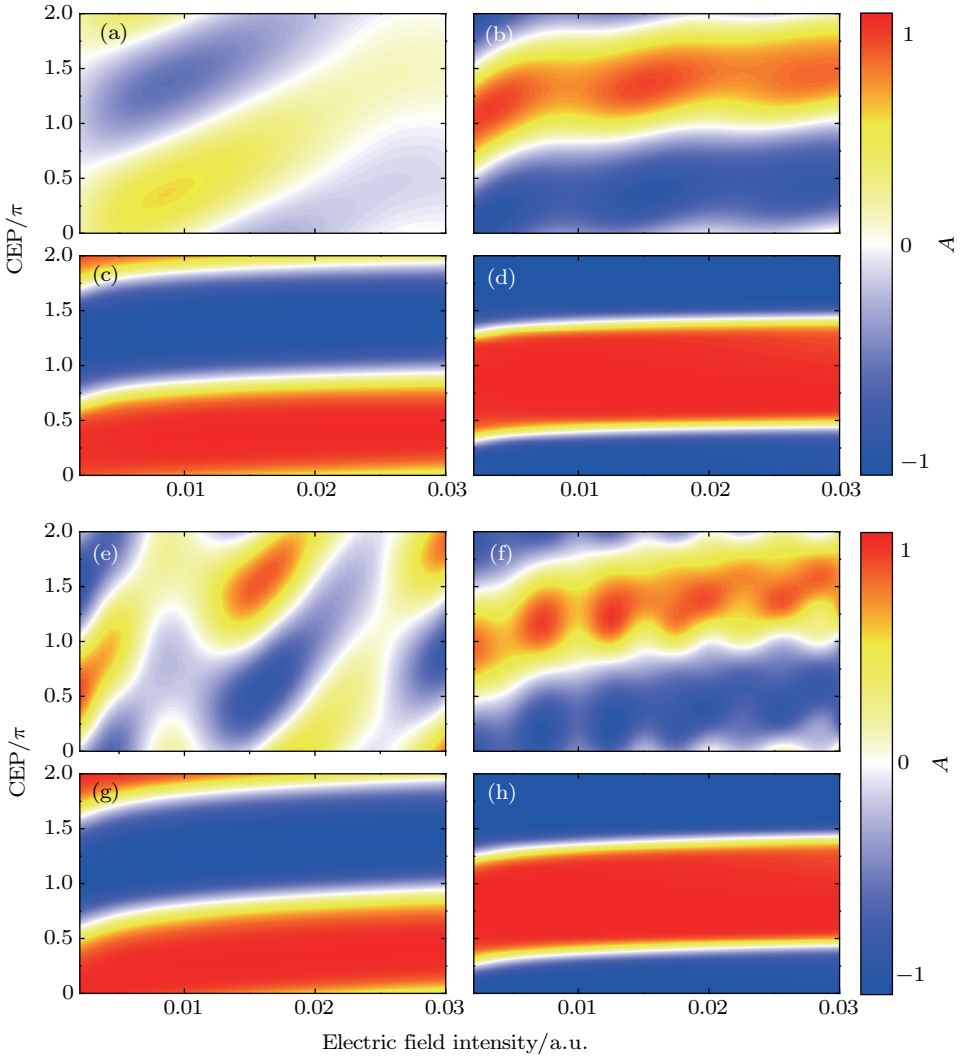


Fig. 6. (color online) The LAP calculated in the three-dimensional TDSE as function of the CEP and the electric field intensity of the probe pulse with different wavelengths: (a) 800 nm, (b) 2000 nm, (c) 4000 nm, and (d) 8000 nm for H_2^+; (e) 2000 nm, (f) 4000 nm, (g) 8000 nm, and (h) 16000 nm for T_2^+.

4. Conclusion

We investigate the wavelength dependence of the electron localization in the UV-pump-probe scheme. An effective analytical method is established to estimate the localization probability by analyzing several zero crossings. The analytical calculation reveals that this method can be used to predict the electron localization quantitatively. A stable zone with respect to the laser intensity and the CEP will be reached by adopting a mid-infrared or terahertz probe wavelength, which satisfies the inequality $\tau_i \omega_{probe}/\pi \ll 1$. Finally, the results calculated by the three-dimensional TDSE show the correctness of our conclusion. Critical probe wavelength λ_c to reach at the stable zone is predicted to be 3000 nm for H_2^+ and 8000 nm for T_2^+. The longer critical wavelength of the heavier isotopomer is ascribed to the slower nuclear motion. To be noted, high electron localization probability does not mean the reaching of the stable zone, whereas the stable zone definitely leads to a high localization probability and provides an easy-to-implement strategy to manipulate the dissociation without being concerned much about the laser parameters except the probe wavelength. We expect the results in this work to be observed in an experiment in the near future.

References

[1] Zewail A H 2000 *J. Phys. Chem. A* **104** 5660
[2] Brixner T and Gerber G 2003 *Chem. Phys. Chem.* **4** 418
[3] González-Castrillo A, Palacios A, Bachau H and Martín F 2012 *Phys. Rev. Lett.* **108** 063009
[4] Niikura H, Villeneuve D M and Corkum P B 2004 *Phys. Rev. Lett.* **92** 133002
[5] Kremer M, Fischer B, Feuerstein B, de Jesus V L B, Sharma V, Hofrichter C, Rudenko A, Thumm U, Schröter C D, Moshammer R and Ullrich J 2009 *Phys. Rev. Lett.* **103** 213003
[6] Singh K P, He F, Ranitovic P, Cao W, De S, Ray D, Chen S, Thumm U, Becker A, Murnane M M, Kapteyn H C, Litvinyuk I V and Cocke C L 2010 *Phys. Rev. Lett.* **104** 023001
[7] Sansone G, Kelkensberg F, Perez-Torres J F, Morales F, Kling M F, Siu W, Ghafur O, Johnsson P, Swoboda M, Benedetti E, Ferrari F, Lepine F, Sanz-Vicario J L, Zherebtsov S, Znakovskaya I, L'Huillier A, Ivanov M Y, Nisoli M, Martin F and Vrakking M J J 2010 *Nature* **465** 763
[8] Roudnev V, Esry B D and Ben-Itzhak I 2004 *Phys. Rev. Lett.* **93** 163601
[9] Kling M F, Siedschlag Ch, Verhoef A J, Khan J I, Schultze M, Uphues Th, Ni Y F, Uiberacker M, Drescher M, Krausz F and Vrakking M J J 2006 *Science* **312** 246
[10] Liu K, Hong W, Zhang Q and Lu P 2011 *Opt. Express* **19** 26359
[11] Ray D, He F, De S, Cao W, Mashiko H, Ranitovic P, Singh K P, Znakovskaya I, Thumm U, Paulus G G, Kling M F, Litvinyuk I V and Cocke C L 2009 *Phys. Rev. Lett.* **103** 223201
[12] Lan P, Takahashi E J and Midorikawa K 2012 *Phys. Rev. A* **86** 013418
[13] Liu K, Zhang Q and Lu P 2012 *Phys. Rev. A* **86** 033410
[14] He F, Becker A and Thumm U 2008 *Phys. Rev. Lett.* **101** 213002
[15] He F, Ruiz C and Becker A 2007 *Phys. Rev. Lett.* **99** 083002
[16] Fischer B, Kremer M, Pfeifer T, Feuerstein B, Sharma V, Thumm U, Schröter C D, Moshammer R and Ullrich J 2010 *Phys. Rev. Lett.* **105** 223001
[17] Anis F and Esry B D 2012 *Phys. Rev. Lett.* **109** 133001
[18] Niikura H, Corkum P B and Villeneuve D M 2003 *Phys. Rev. Lett.* **90** 203601
[19] Jia Z, Zeng Z, Li R, Xu Z and Deng Y 2014 *Phys. Rev. A* **89** 023419
[20] Lu R F, Zhang P Y and Han K L 2008 *Phys. Rev. E* **77** 066701
[21] Xue S, Du H C, Xia Y and Hu B T 2015 *Phys. Rev. A* **92** 013420
[22] Charron E, GiustiSuzor A and Meis F H 1995 *J. Chem. Phys.* **103** 7359
[23] Mulliken R S 1939 *J. Chem. Phys.* **7** 20
[24] He F 2012 *Phys. Rev. A* **86** 063415
[25] Du H C, Wen Y Z, Wang X S and Hu B T 2014 *Chin. Phys. B* **23** 033202
[26] Xue S, Du H C, Xia Y and Hu B T 2015 *Chin. Phys. B* **24** 054210
[27] Feit M D, Fleck J A and Steiger A 1982 *J. Comput. Phys.* **47** 412
[28] Thachuk M, Ivanov M Y and Wardlaw D M 1996 *J. Chem. Phys.* **105** 4094
[29] Thachuk M, Ivanov M Y and Wardlaw D M 1998 *J. Chem. Phys.* **109** 5747
[30] Herzberg G, Longuet-Higgins H C 1963 *Discuss. Faraday Soc.* **35** 77
[31] Longuet-Higgins H C 1975 *Proc. Roy. Soc. Ser. A* **344** 147
[32] Dietrich P, Ivanov M Y, Ilkov F A and Corkum P B 1996 *Phys. Rev. Lett.* **77** 4150
[33] Yu C, He H, Wang Y, Shi Q, Zhang Y and Lu R 2014 *J. Phys. B: At. Mol. Opt. Phys.* **47** 055601
[34] Frasinski L J, Posthumus J H, Plumridge J and Codling K 1999 *Phys. Rev. Lett.* **83** 3625